Research Square

Preprints are preliminary reports that have not undergone peer review.
They should not be considered conclusive, used to inform clinical practice,
or referenced by the media as validated information.

Shielding effect enables ultrafast ion transfer through nanoporous membrane for highly energy-efficient electrodialysis

Jiuyang Lin
Fuzhou University
Wenyuan Ye
Fujian Agriculture and Forestry University
Shuangling Xie
Fuzhou University
Jiale Du
Fuzhou University
Riri Liu
Fuzhou University
Dong Zou
Hanyang University
Xiangyu Chen
Fuzhou University
Zijian Yu
Fuzhou University
Shengqiong Fang
Fuzhou University
Elisa Yun Mei Ang
Singapore Institute of Technology
William Toh
Nanyang Technological University
Dan Dan Han
Hunan University
Teng Yong Ng
Nanyang Technological University
Dong Han Seo
Korea Institute of Energy Technology
Shuaifei Zhao
Deakin University
Bart Van der Bruggen

KU Leuven

Ming Xie (m.xie2@bath.ac.uk)

University of Bath https://orcid.org/0000-0003-2729-9746

Young Moo Lee

Hanyang University https://orcid.org/0000-0002-5047-3143

Article

Keywords:

Posted Date: August 12th, 2022

DOI: https://doi.org/10.21203/rs.3.rs-1894364/v1

License: This work is licensed under a Creative Commons Attribution 4.0 International License.
Read Full License

Shielding effect enables ultrafast ion transfer through nanoporous membrane for highly energy-efficient electrodialysis

Jiuyang Lin,[1]†* Wenyuan Ye,[2]†* Shuangling Xie,[1] Jiale Du,[1] Riri Liu,[1] Dong Zou,[3] Xiangyu Chen,[1] Zijian Yu,[1] Shengqiong Fang,[1] Elisa Yun Mei Ang,[4] William Toh,[5] Dan Dan Han,[6] Teng Yong Ng,[5] Dong Han Seo,[7] Shuaifei Zhao,[8] Bart Van der Bruggen,[9] Ming Xie,[10]* Young Moo Lee[3]*

† These authors contributed equally to this work.
* Corresponding authors: linjiuyang@126.com (J.L.); ye0508@126.com (W.Y.); m.xie2@bath.ac.uk (M.X.); ymlee@hanyang.ac.kr (Y.M.L.)

[1] College of Environment and Safety Engineering, Fuzhou University, Fuzhou 350116, China

[2] Fujian Provincial Key Laboratory of Soil Environmental Health and Regulation, College of Resources and Environment, Fujian Agriculture and Forestry University, Fuzhou 350002, China

[3] Department of Energy Engineering, College of Engineering, Hanyang University, Seoul, 04763, Republic of Korea

[4] Engineering Cluster, Singapore Institute of Technology, 10 Dover Drive Singapore 138683, Singapore

[5] School of Mechanical and Aerospace Engineering, Nanyang Technological University, 50 Nanyang Avenue, Singapore, 639798, Singapore

[6] College of Mechanical and Vehicle Engineering, Hunan University, Changsha 410082, China

[7] Institute of Energy Materials & Devices, Korea Institute of Energy Technology (KENTECH), Naju, Republic of Korea

[8] Deakin University, Geelong, Institute for Frontier Materials, VIC 3216, Australia

[9] Department of Chemical Engineering, Process Engineering for Sustainable Systems (ProcESS), KU Leuven, Celestijnenlaan 200F, B-3001 Leuven, Belgium

[10] Department of Chemical Engineering, University of Bath, Bath, BA2 7AY, United Kingdom

Abstract

A key to sustainable management of hypersaline organic-rich wastewaters is to precisely fractionate organic components and inorganic salts (NaCl) as individual resources. Conventional nanofiltration and electrodialysis processes suffer from membrane fouling and compromise the fractionation efficacy. Here, we develop a thin-film composite nanoporous membrane (NPM) via co-deposition of dopamine and polyethyleneimine as a highly anion-conducting membrane (ACM). Experimental results and molecular dynamics simulations show that co-deposition of dopamine and polyethyleneimine effectively tailors the membrane surface properties, intensifying the charge shielding effect and enabling ultrafast anion transfer for highly efficient electrodialysis. The resulting NPM exhibits unprecedented electrodialytic fractionation of organics and NaCl (>99.3% desalination efficiency; >99.1% organics recovery) with negligible membrane fouling, dramatically outperforming state-of-the-art anion exchange membranes. Our study sheds light on facile design of high-performance ACMs and associated new mass transport mechanisms in electrodialytic separation, paving the way for sustainable management of complex waste streams.

Introduction

To advance net-zero carbon emission for a circular economy, current wastewater treatment processes urgently need a paradigm shift from conventional contaminant removal to resource

recovery, e.g., energy, nutrients, biomass and other high value-added by-products that are beyond water reclamation by reverse osmosis (1-5). One grand challenge in wastewater treatment is the management of hypersaline organic-rich waste streams produced in a wide range of industrial sectors, such as textile processing, tanneries, food processing, the oil & gas industry, paper mills and pharmaceutical manufacturing (6-9). Therefore, it is important to effectively fractionate organic and inorganic salts (e.g., NaCl) using innovative and advanced separation technology to sustainably recover precious resources from these hypersaline organic-rich waste streams (10).

Membrane-based separation technologies offer opportunities to effectively manage these hypersaline organic-rich waste streams. For instance, nanofiltration is among the most widely used pressure-driven membrane technologies to sieve organics with molecular weights of 200-1000 Da and inorganic salts from the hypersaline organic-rich waste streams based on the synergistic effects of size exclusion and electrostatic repulsion using the nanoporous thin-film composite (TFC) membranes, which retain the organics but partially allow the transmission of inorganic salts (11-16). However, the elevated osmotic pressure, membrane fouling, and cake-enhanced concentration polarization experienced in the pressure-driven nanofiltration process induces significant membrane flux decline, thereby minimizing the separation efficiency of the organic and inorganic salts (17-19). Additionally, the pressure-driven nanofiltration-diafiltration procedure should be implemented with high consumption of pure water to achieve the fractionation of organic and inorganic salts, which inevitably suffers from a considerable loss of the target organics and thus reduces the system productivity (10, 20).

As an alternative approach to nanofiltration, electrodialysis is proposed as a route for desalinating the hypersaline organic-rich wastewaters, which allows cations and anions to be transferred through cation exchange membranes (CEMs) and anion exchange membranes (AEMs) under a direct current electric field (21-23). Nevertheless, most of the organic compounds with negative charges in the hypersaline organic-rich wastewaters migrate to the AEMs via electrostatic attraction, which escalates the membrane fouling during the electrodialysis process (24-26), significantly limiting the transfer efficiency of the anions and jeopardizing the fractionation of the organic and inorganic salts.

By integrating the technical merits of the pressure-driven nanofiltration (nanoporous membranes) and the electrodialysis process (electro-driven process with low/zero pressure), we herein devised a new electro-driven membrane system using TFC nanoporous polyamide (PA) membranes (with a molecular weight cutoff (MWCO) of 200-1000 Da) as anion conducting membranes (ACMs) to replace the AEMs used in conventional electrodialysis. This strategy both alleviates the membrane fouling and accelerates the ion transfer. Due to the nanoporous structure of the membranes, the anions can migrate through the nano-channels of the TFC PA membranes under a direct electric field. However, nanoporous TFC PA membranes are highly negatively charged and can impede the anion transfer to a great extent through electrostatic repulsion and thus deteriorate the desalination efficiency under the current field. Therefore, it is vital to molecularly tailor the surface properties of the nanoporous PA membranes for intensifying the charge shielding effect, thus enhancing the anion transfer and solute selectivity while effectively separating the organics without fouling. To modulate the membrane surface properties, a bio-inspired polydopamine (PDA)-based coating on PA nanofiltration membrane is proposed as a novel strategy for constructing a multifunctional surface for enhanced membrane performance (27, 28). However, there are limited examples of PDA-coated nanoporous membranes (NPMs) in electro-driven membrane process with applications limited to pressure-driven membrane filtration or superhydrophilic surface modifications (29, 30).

In this study, we present the design of surface-engineered, highly anion-conducting, anti-fouling TFC NPMs featuring a facile co-deposition of dopamine and polyethyleneimine (PEI) for effective electrodialytic fractionation of the organic and inorganic salts from hypersaline organic-rich wastewaters (**Fig. 1A** and **1B**). Co-deposition of dopamine and PEI effectively tunes the surface properties of the PDA/PEI coated TFC NPMs as ACMs, which both enhances the solute selectivity (as is evident from the experimental data) and manifests an ion shielding effect for ultrafast electrodialytic anion transfer as demonstrated by molecular dynamics (MD) simulation. The optimal PDA/PEI coated TFC NPM exhibits over 99.3% desalination efficiency and more than 99.1% recovery of organics for highly effective electrodialytic fractionation of various organics/NaCl mixed solutions. Finally, we show that PDA/PEI coated TFC NPMs are exceptionally stable to achieve impressive fractionation performance with negligible fouling propensity in a 6-cycle electrodialytic separation operation. This highlights the practicability of surface-engineered TFC NPMs as advanced ACMs in one-step electro-driven fractionation of the organic and inorganic salts from complex hypersaline organic-rich wastewaters for a sustainable circular economy.

Results

Design and characterization of highly anion-conducting TFC NPMs

A loose poly(piperazine amide) thin-film composite (TFC) NPM with a MWCO of 682±17 Da was used as the substrate for fabrication of highly anion-conductive TFC NPMs via co-deposition of dopamine and PEI at pH=8.5 (Fig. 1A). The coated TFC NPMs were exposed to the dopamine/PEI solution at different durations, i.e., 6, 12, 18, 24, 30 and 36 h, and were denoted as NPM-1, NPM-2, NPM-3, NPM-4, NPM-5, and NPM-6, respectively. Meanwhile, the loose TFC NPM substrate was referred to as NPM-0 and was used as a control. The surface color of the coated TFC membranes changed from a white pattern to a light-yellow pattern and finally to a brown pattern (**Fig. S1**), demonstrating the successful and homogeneous polymerization of dopamine and PEI on the membrane surfaces. This was further confirmed by scanning electron microscopy images (**Fig. S2**). X-ray photoelectron spectroscopy (XPS) analysis proved that the co-deposition of dopamine and PEI on the loose NPM substrate was induced through Schiff base or/and Michael addition reactions (**Fig. S3**). Such a PDA/PEI complex coating enables an increase in the thickness of selective layer for the PDA/PEI coated NPMs from 87.5±8.5 nm (NPM-0) to 135.0±12.6 nm (NPM-6), as demonstrated by atomic force microscopy (AFM) measurements (**Fig. S4** and **Fig. S5**).

Furthermore, the surface properties (i.e., hydrophilicity, surface charges, specific areal electric resistance and pore size) of the PDA/PEI coated NPMs can be precisely tuned via co-deposition of dopamine and PEI on the loose NPM substrate (**Fig. 1E-1H**). In particular, the surfaces of the coated NPMs become more hydrophilic and less negatively charged (**Fig. 1E** and **1F**) due to the intercalation of the PEI molecules with positive charges through co-polymerization with dopamine. Such a PDA/PEI complex coating can minimize the specific areal electric resistance of the coated NPMs through reduced surface negative charge density (**Fig. 1G**). As expected, the specific areal electric resistance of the coated TFC NPMs was reduced from 10.47±0.43 (NPM-0) to 5.69±0.13 $\Omega \cdot cm^2$ (NPM-6) after a 36-h deposition of the PDA/PEI complex layer, which is beneficial for enhanced ion conductivity under an electric field. Simultaneously, the pore size of the coated TFC NPMs was significantly reduced since the PDA/PEI complex coating can sufficiently bridge the cavity structure of the loose NPM substrate, which can enhance the retention of organics (as reflected by the reduction in MWCO and effective mean pore size in **Fig. 1H**, **Fig. S6** and **Table S3**). This change in surface properties endow the PDA/PEI coated TFC NPMs with enhanced selectivity of the organics over inorganic salts (i.e., NaCl).

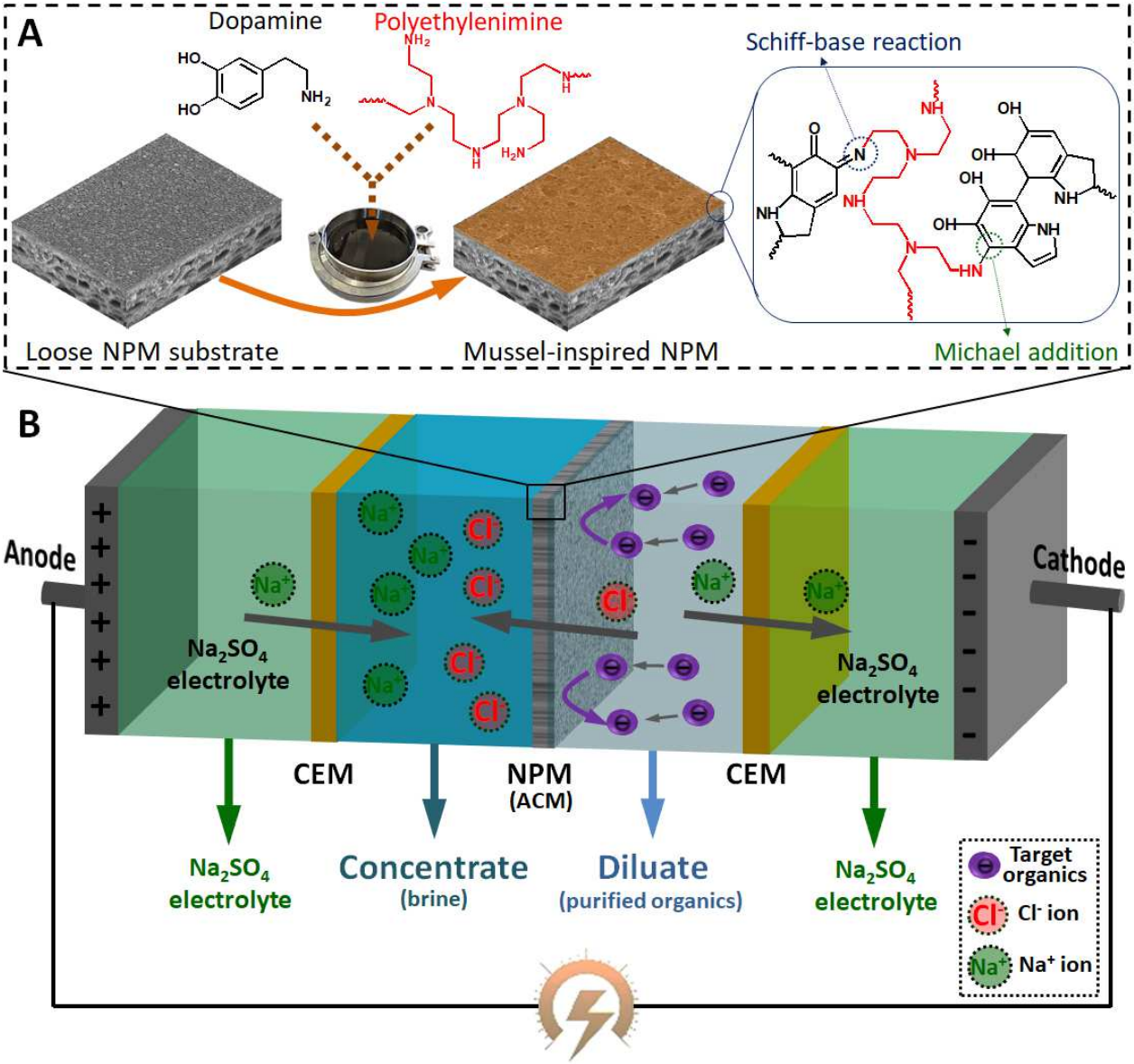
A
Dopamine
Polyethylenimine
Schiff-base reaction
Loose NPM substrate
Mussel-inspired NPM
Michael addition
B
Anode
Cathode
Na_2SO_4 electrolyte
Na_2SO_4 electrolyte
CEM
NPM (ACM)
CEM
Na_2SO_4 electrolyte
Concentrate (brine)
Diluate (purified organics)
Na_2SO_4 electrolyte
Target organics
Cl^- ion
Na^+ ion

142

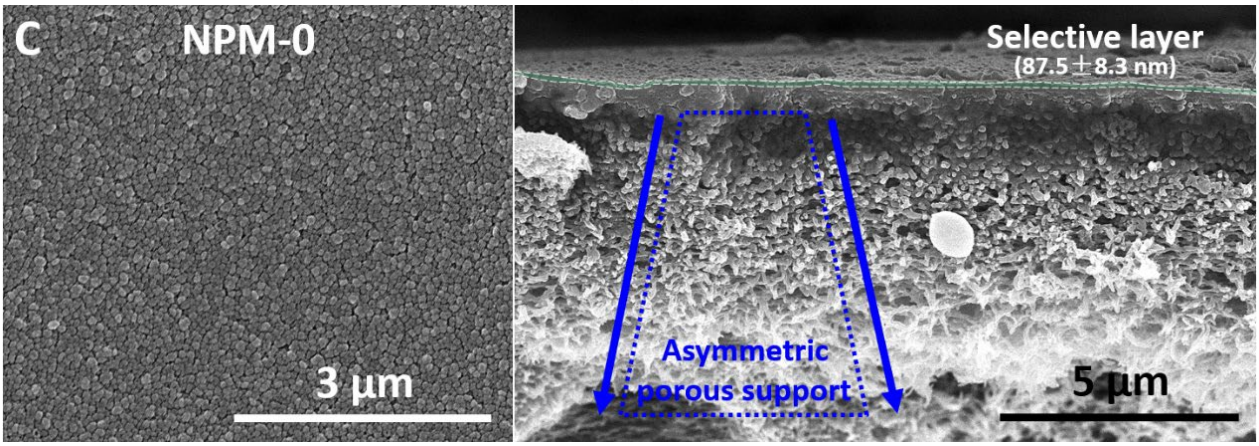
C
NPM-0
3 μm
Selective layer
(87.5±8.3 nm)
Asymmetric porous support
5 μm

143

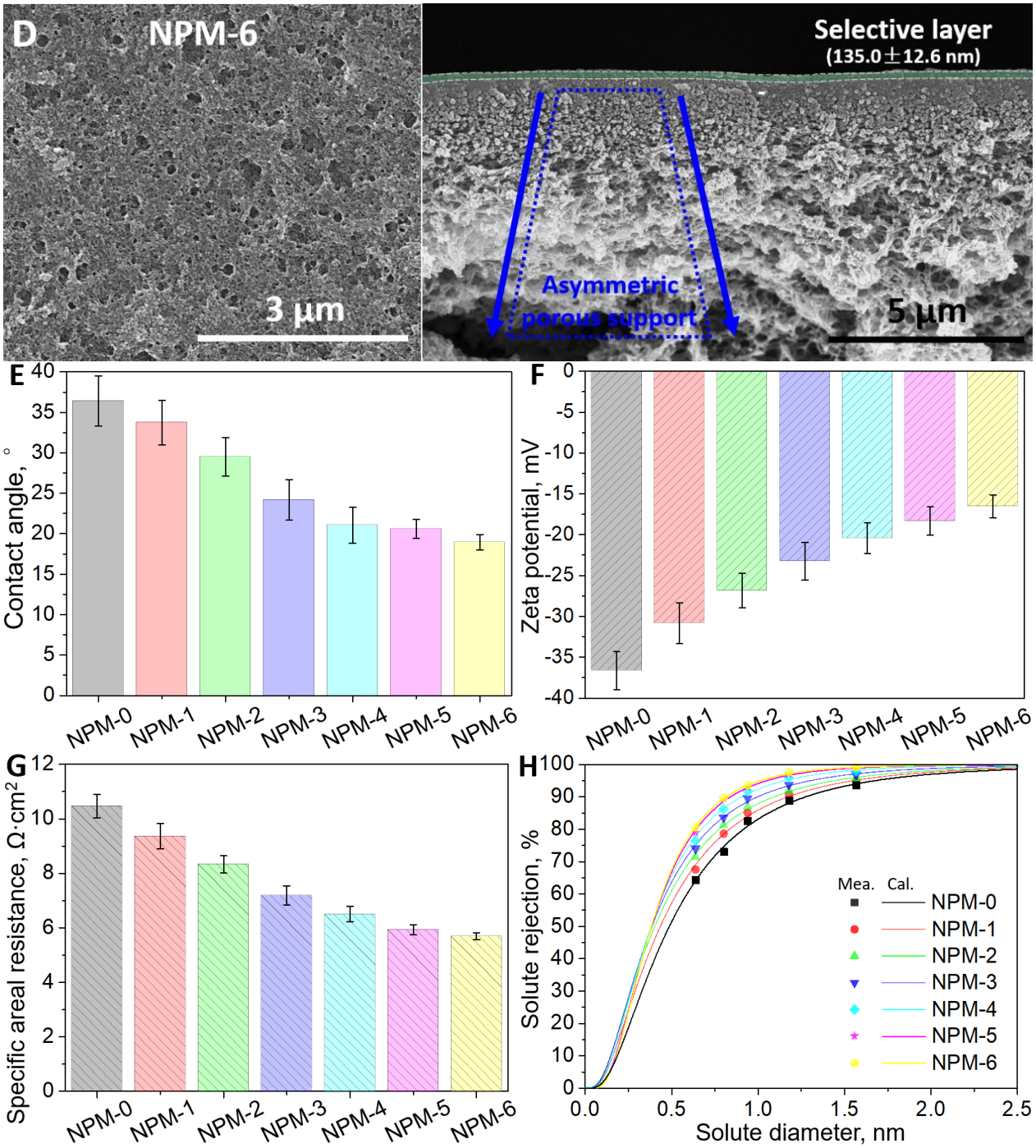

Fig. 1. Design and characterization of surface engineered TFC NPMs as ACMs for electrodialytic fractionation of organics and NaCl. (**A**) Schematic diagram of dopamine-based bio-inspired coating of TFC NPM, (**B**) stack configuration of novel electro-driven separation process using the PDA/PEI coated NPMs as ACMs for one-step electrodialytic fractionation of organics and NaCl, (**C**) surface and cross-sectional SEM images of the loose TFC NPM substrate, (**D**) surface and cross-sectional SEM images of the TFC NPM after 36-h PDA/PEI coating (NPM-6), (**E**) surface hydrophilicity of the TFC NPMs, (**F**) zeta potential of the TFC NPMs, (**G**) specific areal electric resistance of the TFC NPMs, (**H**) relationship between molecular weights of poly(ethylene glycol) polymers and their rejection for the TFC NPMs.

Pressure-driven separation performance of the coated TFC NPMs

Pressure-driven filtration was performed to illustrate the solute selectivity of the PDA/PEI coated NPMs between inorganic salts (i.e., NaCl) and organics. In this study, four antibiotics, including

ceftriaxone sodium, cefotaxime sodium, carbenicillin disodium, and ampicillin sodium, were selected as the model organics. The rejection of antibiotics for the PDA/PEI coated NPMs increased when the coating duration was extended (**Fig. S7A**), which is ascribed to the reduction in pore size of the PDA/PEI coated NPMs, which enhances the organic rejection via a size exclusion effect. For instance, the NPM-6 membrane exhibited rejection of 98.5±0.2% to ampicillin sodium, markedly outperforming the pristine loose NPM-0 substrate (88.9±0.5%). Conversely, the rejection of NaCl for the PDA/PEI coated NPMs unexpectedly decreased with increasing coating duration (**Fig. S7B**). This could be attributed to the reduction in negative surface charge density of the coated NPMs (reflected by the change in zeta potential in **Fig. 1F**), leading to a diminished electrostatic repulsion for fast NaCl transmission (31-33).

Both organic and inorganic salts (i.e., NaCl) co-exist in real hypersaline organic-rich solutions. The presence of inorganic salts would significantly affect the separation behavior of the TFC NPMs, which enhances the shielding effect for reduced solute retention (7, 34). Specifically, the rejection of organics for the pristine loose NPM substrate (i.e., NPM-0) significantly decreased with increasing NaCl concentration, yielding a reduced selectivity between NaCl and antibiotics in the antibiotic/NaCl mixed solutions as feed (**Fig. 2A**). After coating of the PDA/PEI complex layer, the coated TFC NPMs exhibited increasing rejection toward the organics in the same antibiotic/NaCl mixed solutions (**Fig. 2B** and **Fig. S8**). The deleterious impact of the presence of NaCl on the rejection of organics was minimized for the PDA/PEI coated NPMs with a 36-h coating duration (i.e., NPM-6). The rejection of all the antibiotics for the NPM-6 membrane was marginally diminished with increasing NaCl concentrations since the size exclusion effect of the NPM-6 membrane was maximized with a remarkable reduction in its pore sizes. This enabled an impressive increase in selectivity of NaCl and antibiotics for their potential effective fractionation (**Fig. 2C**). For instance, the selectivity of NaCl and ampicillin sodium in the antibiotic/NaCl mixed solution through the NPM-6 membrane reached 27.4, which was much higher than that (i.e., 5.0) of the pristine loose NPM-0 substrate during the pressure-driven nanofiltration procedure (**Fig. 2C**).

Although the PDA/PEI-coated NPMs showed enhanced selectivity between NaCl and antibiotics, a constant-volume nanofiltration-based diafiltration procedure using the NPM-6 membrane should be implemented for fractionation of antibiotics and NaCl from the antibiotic/NaCl mixed solutions (**Fig. 2D** and **Fig. S9**). The concentration of NaCl in all the antibiotic/NaCl mixed solutions significantly decreased with increasing diavolume number during diafiltration. This is because the low overall rejection of NaCl (<30%) for the NPM-6 membrane allowed fast penetration of NaCl through the membrane (**Fig. S10A-S13A**). When the diavolume number increased to 5.9-6.0, the concentration of NaCl in all the antibiotic/NaCl mixed solutions was reduced from ~ 11.9 $g \cdot L^{-1}$ to ~ 0.08 $g \cdot L^{-1}$, resulting in a desalination efficiency of 99.3%-99.4% (**Table S4**). On the other hand, the NPM-6 membrane with smaller pore size can effectively retain the antibiotics even after diafiltration of the antibiotic/NaCl mixed solutions. However, as the diavolume number increased, the antibiotics were still able to penetrate through the NPM-6 membrane along with the nanofiltration permeate. For antibiotics with a lower molecular weight (e.g., ampicillin sodium), a moderate amount of the antibiotics was transported from the feed to the permeate, even though the NPM-6 membrane exhibited rejections of >96% to the antibiotics. Consequently, the loss of ceftriaxone sodium, cefotaxime sodium, carbenicillin disodium and ampicillin sodium from the feed to the permeate side reached 4.18%, 6.27%, 8.98%, and 11.47% (**Fig. S10B-S13B**), respectively. Therefore, the constant-volume nanofiltration-based diafiltration procedure driven by pressure demonstrated insufficient recovery of antibiotics during the fractionation of antibiotics and NaCl from the antibiotic/NaCl mixed solutions (**Table S4**).

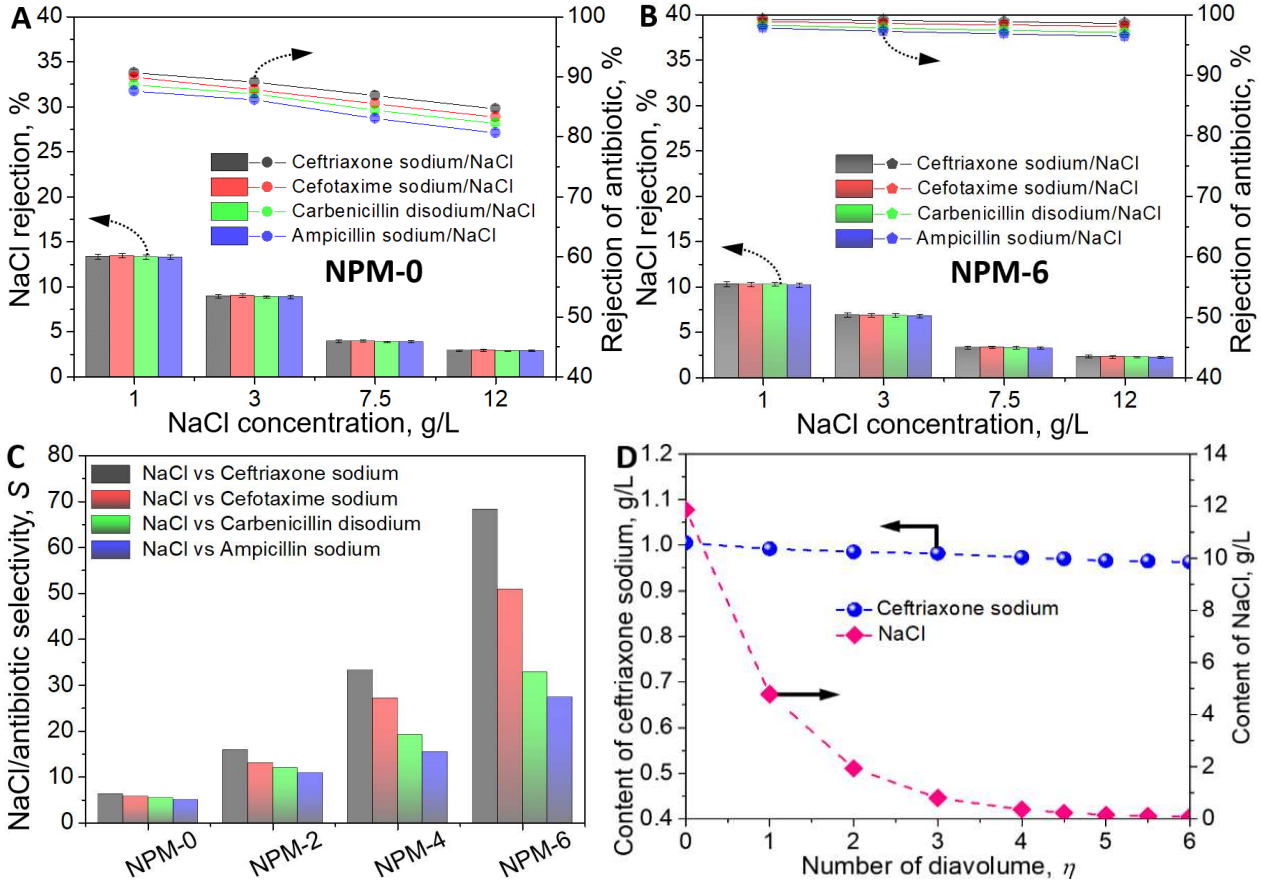

Fig. 2. (**A**, **B**) Rejection of antibiotics and NaCl for the NPM-0 and NPM-6 membranes, respectively, when filtering various antibiotic/NaCl mixed solutions, (**C**) selectivity between NaCl and antibiotic for the NPM-0, NPM-2, NPM-4 and NPM-6 membranes when filtering various antibiotic/NaCl mixed solutions with a NaCl concentration of 12 $g \cdot L^{-1}$, (**D**) content of antibiotic and NaCl in the feed during the constant-volume nanofiltration-based diafiltration using the NPM-6 membrane for fractionation of antibiotics and NaCl from a ceftriaxone sodium/NaCl mixed solution.

Electro-driven separation performance of the coated TFC NPMs as ACMs

The PDA/PEI coated NPMs were used as ACMs to replace the AEMs in the conventional electrodialysis for evaluating their electro-driven separation performance (**Fig. 3**). During the electro-driven membrane-based separation, sufficient desalination of the pure NaCl solutions can be achieved using the PDA/PEI coated NPMs as ACMs (**Fig. 3A**). For instance, the NPM-6 membrane yielded a desalination efficiency of 99.5% for the pure NaCl solution with a minimal energy consumption of 5.86±0.10 $kWh \cdot kg^{-1}$ during 124 min of operation (**Fig. 3B** and **3C**), which was comparable to commercial AEMs (**Fig. S14B**, **S14D** and **S14E**). This demonstrates the impressive anion transfer capacity of the PDA/PEI coated NPMs for desalination (**Fig. 3D**). The remarkable anion transfer enhancement of the PDA/PEI coated TFC NPMs was mainly attributed to two factors: (i) sufficient nano-channels and short ion diffusion pathways caused by the intrinsically thin selective layer of the PDA/PEI coated TFC NPMs that enable effective anion transfer under the electric field; (ii) the reduced negative charge density of the PDA/PEI coated TFC NPMs intensifies the shielding effect and thus lowers the energy barrier (i.e., electrostatic repulsion) between anions and the membrane surface for anion transfer. Although commercial AEMs with a non-porous structure generally have abundant positively-charged quaternary ammonium group sites, their thickness is in the hundreds of micrometers, which provides a longer ion diffusion pathway for anion transfer (**Fig. S14C**). Therefore, such an improvement in anion

conductivity of the PDA/PEI coated TFC NPMs provides an important conceptual framework for the facile design of cost-effective ACMs.

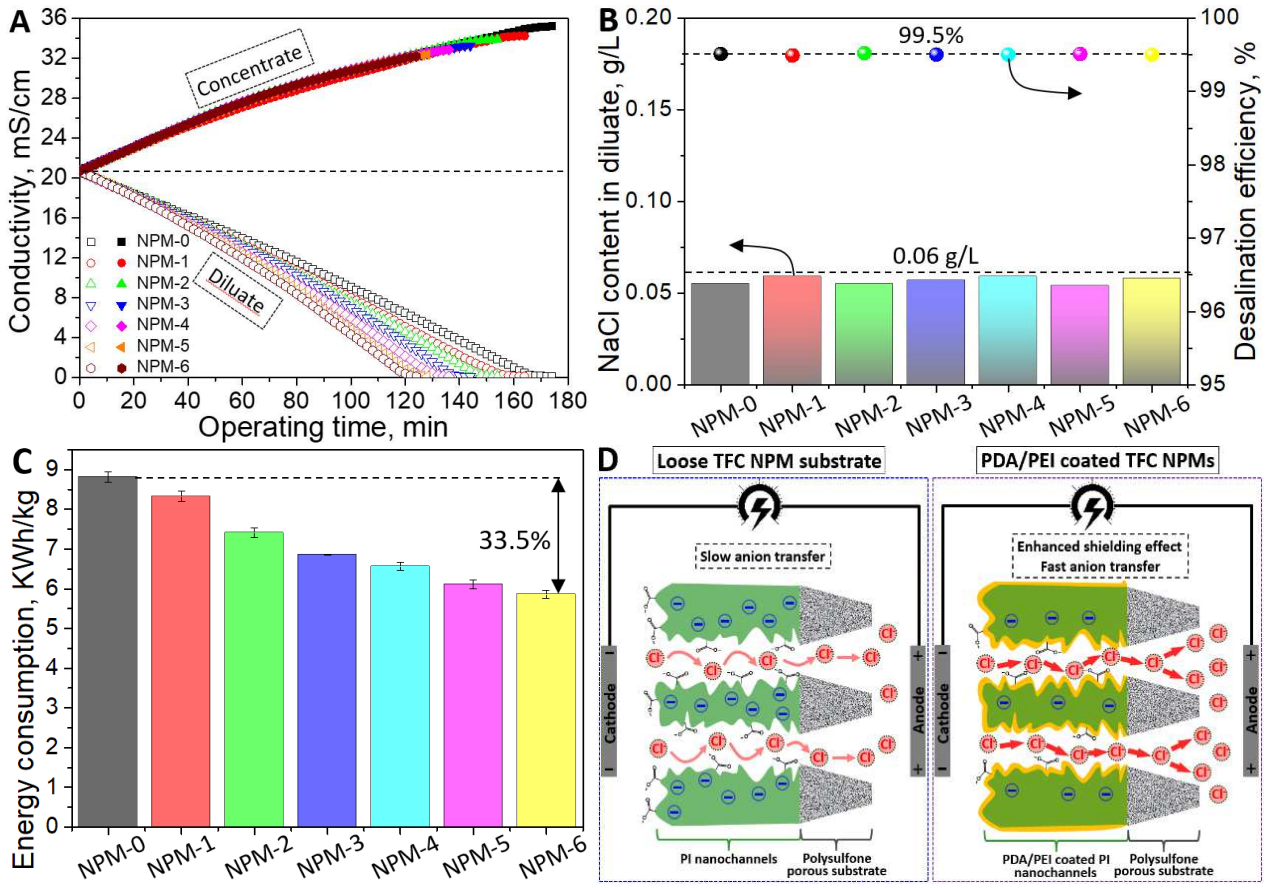

Fig. 3. Electrodialytic separation performance of the PDA/PEI-coated TFC NPMs in pure NaCl solution (about 12.0 g·L^{1}) at a current of 0.5 A. (**A**) Evolution of conductivity in both concentrate and diluate, (**B**) NaCl concentration in the diluate and desalination efficiency, (**C**) energy consumption, (**D**) illustration of anion transfer pathway through the TFC NPMs during the electrodialytic separation.

In addition, we examined the fractionation efficacy of the PDA/PEI coated TFC NPMs (i.e., NPM-6) in the antibiotic/NaCl mixed solutions under an electric field. Sufficient anion transfer capacity imparted the NPM-6 membrane with a desalination efficiency of >99.3% for all the antibiotic/NaCl mixed solutions (**Fig. 4A-4D**). On the other hand, only a trace amount of organics (<10 ppm) passed to the concentrate side, suggesting sufficient fractionation of all the antibiotics (i.e., ceftriaxone sodium, cefotaxime sodium, carbenicillin disodium, and ampicillin sodium) and NaCl. Unprecedentedly high recovery efficiencies (>99.1%) of all the antibiotics were obtained from the antibiotic/NaCl mixed solutions (**Table 1**) during the electro-driven separation. Therefore, the PDA/PEI coated TFC NPMs with a thin nanoporous layer offer both nano-channels for effective, unperturbed anion transfer, and they substantially retain organics via an enhanced size exclusion effect, leading to a one-step fractionation of the organics and NaCl under an electric field. Furthermore, such an electro-driven separation process using the surface-engineered TFC NPMs (i.e., NPM-6) as ACMs markedly outperformed the pressure-driven diafiltration process using the NPM-6 membrane as a nanofiltration membrane (**Table S4**) for fractionation of the organics and NaCl in terms of organic recovery and water consumption.

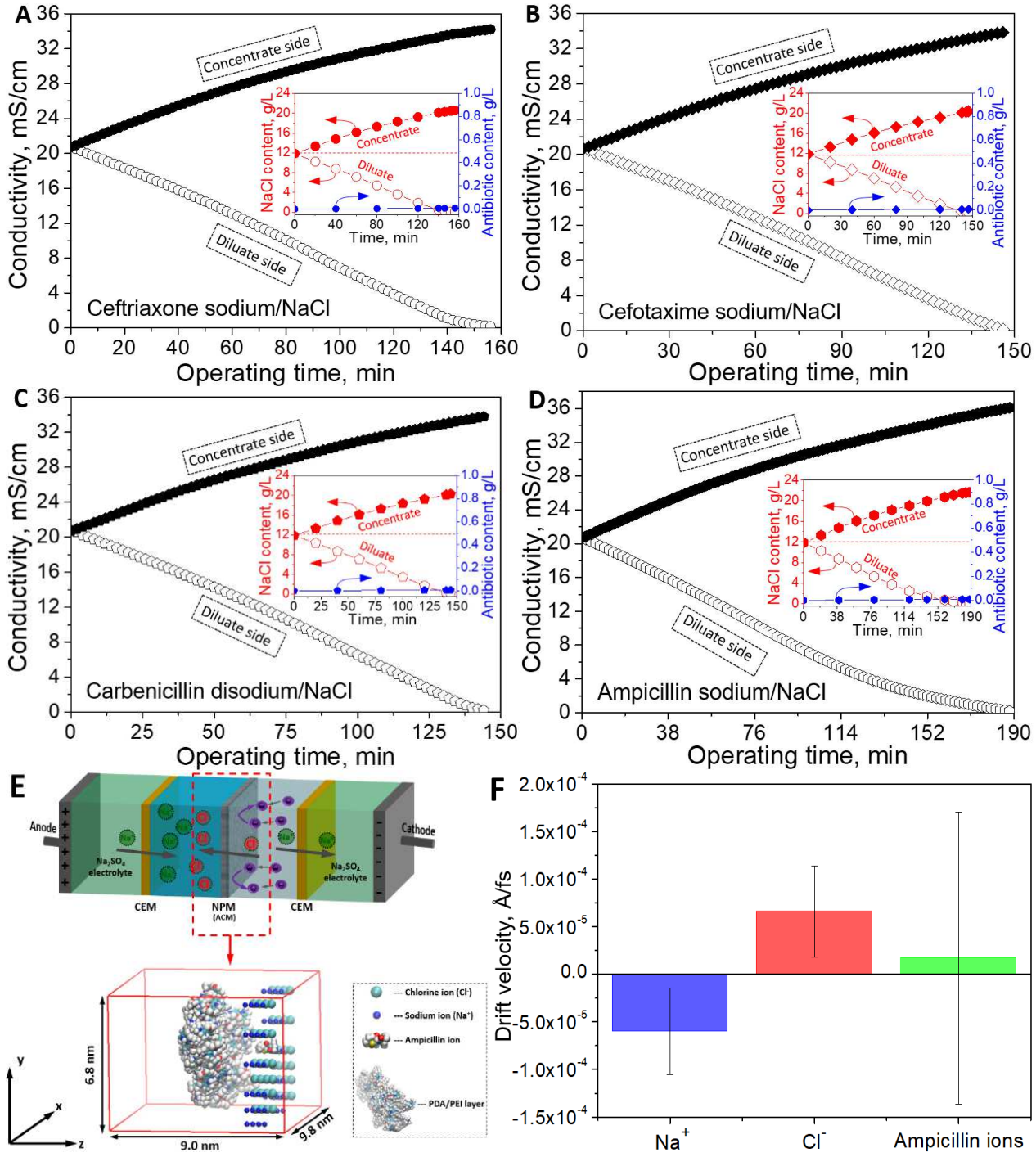

Fig. 4. (**A-D**) Evolution of conductivity in the concentrate and diluate during fractionation of antibiotic and NaCl in the ceftriaxone sodium/NaCl, cefotaxime sodium/NaCl, carbenicillin disodium/NaCl and ampicillin sodium/NaCl mixed solutions, respectively, by electro-driven process using the NPM-6 membrane at a current of 0.5 A (inset: content of NaCl in both concentrate and diluate and content of antibiotic in the concentrate), (**E**) details of the MD simulation domain (note that water molecules are not shown in the simulation domain for clarity), (**F**) drift velocity of Na^+, Cl^- and ampicillin ions with samples collected at every 200-fs interval for the last 0.2 ns of the MD system run.

Table 1. Performance overview of electro-driven separation process using PDA/PEI coated NPM (i.e., NPM-6) for one-step fractionation of antibiotics and NaCl

Organics/NaCl mixtures	NaCl content in diluate, $g \cdot L^{-1}$	Desalination efficiency, %	Recovery of antibiotics, %
Ceftriaxone sodium/NaCl	0.076	99.36	99.28
Cefotaxime sodium/NaCl	0.08	99.33	99.26
Carbenicillin disodium/NaCl	0.083	99.30	99.21
Ampicillin sodium/NaCl	0.078	99.35	99.11

Fouling propensity of the coated TFC NPMs during electro-driven separation

To challenge long-term viability of the PDA/PEI-coated NPMs for fractionation of the antibiotic/NaCl mixed solutions, the fouling propensity of the NPM-6 membrane based on a six-cycle electro-driven separation operation was investigated (**Fig. 5**). Nearly identical performance in each cycle for fractionation of antibiotics (i.e., ceftriaxone sodium) and NaCl was observed in this six-cycle electro-driven separation operation, featuring the superior long-term stability of TFC NPM with a consistently high desalination efficiency over several cycles (about 99.3%) (**Fig. 5A** and **5B**). Such an extremely low fouling propensity of the NPM-6 membrane was further demonstrated by the modest increase in its specific areal electric resistance after a six-cycle electro-driven separation operation (**Fig. 5B**). In summary, the outstanding overall fractionation performance of the NMP-6 membrane can be explained by its relatively small pore size, which sufficiently retained the organics and impeded the penetration of the organics into the inner pore structure from the blockage of its nano-channels, eventually guaranteeing effective anion transfer and recovery of the organics (>99.2%) (**Fig. 5C** and **5D**). Moreover, the negatively-charged surface of the NPM-6 membrane aided in electrostatic repulsion of the organics to some extent, lowering the fouling propensity.

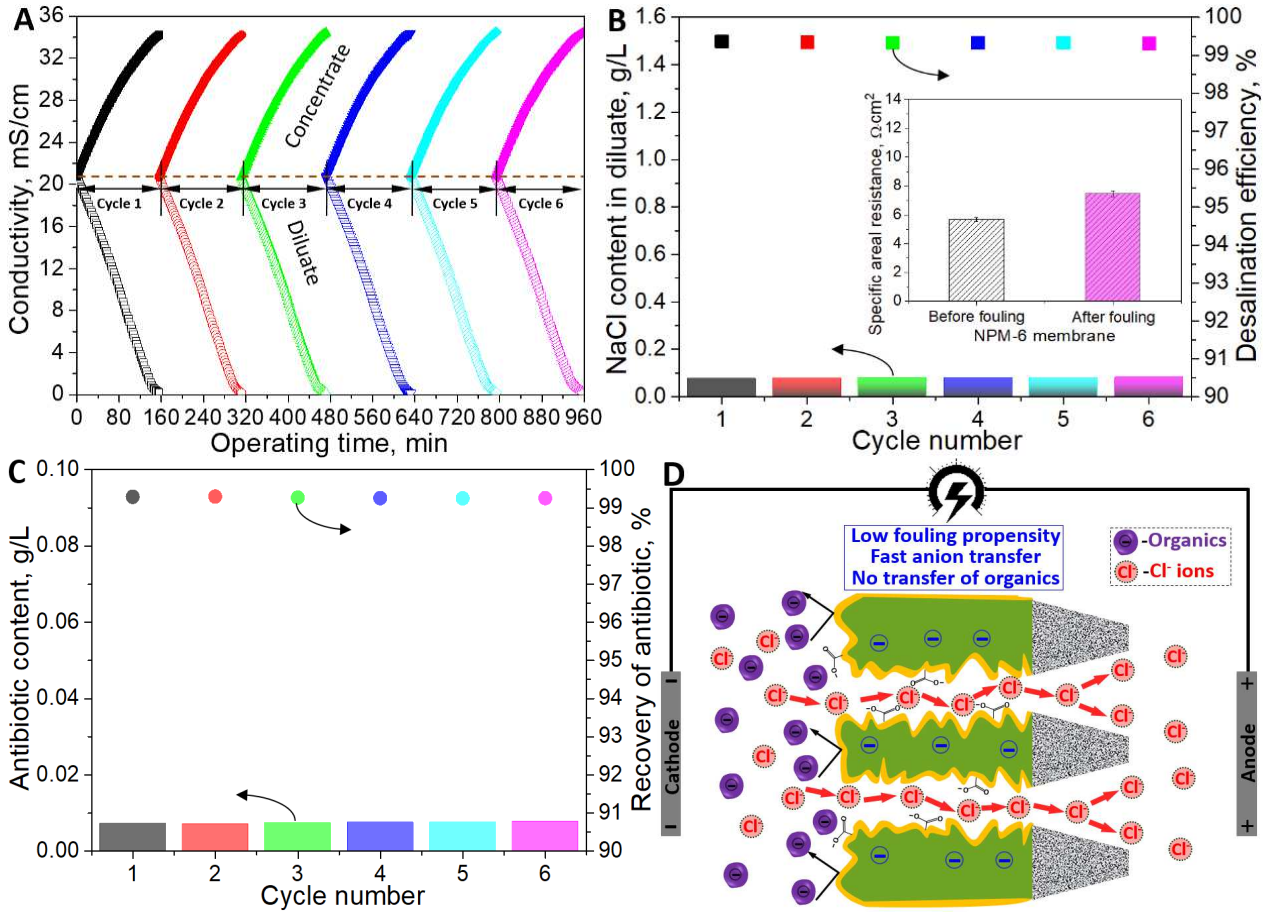

Fig. 5. Six-cycle electrodialytic separation process using the NPM-6 membrane as ACM for fractionation of the ceftriaxone sodium/NaCl mixed solution. (**A**) Evolution of conductivity in the concentrate and diluate, (**B**) content of NaCl in the diluate and its desalination efficiency (inset: specific areal electric resistance of NPM-6 before and after fouling), (**C**) content of ceftriaxone sodium in the concentrate and its recovery rate, (**D**) schematics of anion transfer of the NPM-6 membrane during electrodialytic fractionation of ceftriaxone sodium and NaCl.

Discussion

Unlike the AEMs with positively-charged group sites, the PDA/PEI coated TFC NPMs provide enhanced electrodialytic transfer of anions by intensifying the charge shielding effect. Furthermore, we performed MD simulations of ion transfer to further elucidate the mass transport mechanism of the PDA/PEI coated TFC NPMs in electrodialysis (**Fig. 4E-4F** and **Movies S1-S3**). When the electric field was applied across the PDA/PEI coated TFC NPMs, we observed that Cl^- ions move toward the anode through the PDA/PEI coated NPMs, while Na^+ ions move toward the cathode (**Movies S1** and **S2**). Additionally, the calculated negative drift velocity of Cl^- ions and positive drift velocity of Na^+ ions (**Fig. 4F**) demonstrate the moving direction of Cl^- and Na^+ ions under the electric field. Although there is a weak electrostatic repulsion between the slight negatively-charged PDA/PEI complex layer and negatively-charged Cl^- ions, the applied electric field is sufficiently strong to overcome the electrostatic repulsion, allowing the Cl^- ions to pass through the PDA/PEI complex layer of the coated TFC NPMs. In contrast, ampicillin ions as model organics had a smaller drift velocity of 1.7E-5 Å/fs with a larger standard deviation (i.e., 1.5E-4 Å/fs), implying that ampicillin ions move much more haphazardly and are not oriented toward a fixed pole (**Movie S3**). Therefore, the movement of the ampicillin ions is not significantly influenced by the strong electric field applied. Due to the size exclusion effect, the ampicillin ions can be effectively retained by the PDA/PEI coated NPMs and remain in the diluate side. Consequently, the ampicillin and Cl^- ions could be effectively separated. Therefore, the MD simulation further confirms the superiority of the

electrodialytic separation process using the PDA/PEI coated TFC NPMs as ACMs for effective fractionation of organics and NaCl.

Generally, the conventional electrodialysis units equipped with AEMs are a platform technology for desalination of hypersaline organic-rich solutions. However, the commercial AEMs (i.e., AEM-1) suffered from serious membrane fouling for a six-cycle electrodialytic separation operation during the fractionation of the antibiotics (i.e., ceftriaxone sodium) and NaCl in the antibiotic/NaCl mixed solution (**Fig. S15**). This was mainly attributed to the electrostatic attraction between negatively charged organics (i.e., ceftriaxone ions) and positively-charged quaternary ammonium group sites of the AEMs (**Fig. S15E**), which can both induce pore blockage of the AEMs and substantially reduce the positive charge density of the AEMs (as reflected by remarkable boost in specific areal electric resistance of AEM-1 membrane after fouling in **Fig. S15D**), which impedes the anion transfer. The fouling of the commercial AEM-1 membrane required increased operation duration to remove the inorganic salts (i.e., NaCl) from the feed (i.e., diluate) for each cycle with a reduced desalination efficiency (**Fig. S15A**). Specifically, the desalination efficiency of the commercial AEM-1 membrane declined from 98.01% to 97.50% in the ceftriaxone sodium/NaCl mixed solution after the six-cycle electrodialytic separation operation. Correspondingly, the content of NaCl in the ceftriaxone sodium/NaCl mixed solution was maintained at a level of >0.23 $g \cdot L^{-1}$ at the six-cycle separation operation (**Fig. S15B**). On the other hand, negatively-charged ceftriaxone ions inevitably transferred through the AEM-1 membrane to the concentrate side through electrostatic attraction under the electric field, resulting in the high content of ceftriaxone sodium (>77 $mg \cdot L^{-1}$) in the concentrate side and low antibiotic recovery (<92.3%) (**Fig. S15C**).

Therefore, utilization of bio-inspired PDA/PEI-coated TFC NPMs as ACMs in the electrodialytic separation process can facilitate the efficient one-step fractionation of the organic and inorganic salts (i.e., NaCl) from hypersaline organic-rich solutions containing antibiotics, remarkably outperforming the commercial AEMs. This proof-of-concept study sought to both effectively sieve the organic and inorganic salts for resource recovery from various hypersaline organic-rich waste streams and provide guidelines for facile design of bespoken, cost-effective and high-performance ACMs to replace conventional high-fouling AEMs in the electro-driven separation applications for sustainable management of a complex water matrix.

Methods

Materials and chemicals

A commercial loose poly(piperazine-amide) thin-film composite (TFC) nanoporous membrane (NPM) (MWCO 682±17 Da) was purchased from Guangdong Yinachuan Environmental Technology Co., Ltd. (China) and was used as the substrate for fabrication of advanced anion conducting membranes (ACMs). The commercial cation exchange membrane (i.e., CJMC-3) for cation transfer in electrodialysis was kindly supplied by ChemJoy Polymer Materials Co., Ltd. (China). Four commercial anion exchange membranes (AEMs) were supplied by Guangdong Yinachuan Environmental Technology Co., Ltd. (China), Shandong Tianwei Membrane Technology Co., Ltd. (China), and Fumatech (Germany), which were designated as AEM-1, AEM-2, AEM-3 and AEM-4, respectively. The properties of these commercial AEMs are shown in **Table S1**.

Polyethylenimine (PEI, average molecular weight 600 Da, 99%) and tris(hydroxymethyl) aminomethane (Tris, >99%) were supplied by Shanghai Aladdin Biochemical Technology Co., Ltd. (China). Dopamine hydrochloride (>98%) was supplied from Sigma-Aldrich. These chemicals were used as received for surface coating of the loose nanoporous membrane (NPM). Four antibiotics, i.e., ceftriaxone sodium (molecular weight (MW) 598.5 Da, >98%), cefotaxime sodium

(MW 477.5 Da, 99.5%), carbenicillin disodium (MW 422.4 Da, USP grade), and ampicillin sodium (MW 371.4 Da, USP grade) were purchased from Shanghai Aladdin Biochemical Technology Co., Ltd. (China). NaCl (>99.0%) was supplied from Sigma-Aldrich. Chemicals were used as received without any purification.

Mussel-inspired coating of TFC NPMs

The mussel-inspired coating on the loose TFC NPM substrate was performed by co-deposition of dopamine and PEI as illustrated in **Fig. 1A**. The loose NPM substrate coupon was first loaded in the custom-made round mold, which allowed the membrane surface to stand with its side up. Subsequently, dopamine hydrochloride (2.0 $g \cdot L^{-1}$) and PEI (2.0 $g \cdot L^{-1}$) were homogeneously dissolved in a Tris buffer solution (50 $mmol \cdot L^{-1}$, pH=8.5) by vigorous stirring. Then, the as-prepared dopamine/PEI mixed solution was immediately poured into the mold for mussel-inspired surface coating onto the loose TFC NPM substrate. The co-deposition coating duration was fixed at 0, 6, 12, 18, 24, 30, and 36 h, respectively. The resulting membranes at variable coating durations were denoted as NPM-0 (pristine), NPM-1, NPM-2, NPM-3, NPM-4, NPM-5, and NPM-6, respectively.

Membrane characterization

The surface and cross-sectional morphologies of the membranes were visualized by SEM (NOVA NanoSEM 230; NOVA NanoSEM 450). The surface chemical composition of the membranes was recorded by XPS with Axis Supra+ spectrometer (Kratos Analytical). The selective layer thickness of the membranes was determined by AFM (Agilent 5500, USA), as described in detail in the Supplementary Materials.

The surface hydrophilicity of the membranes was measured using an optical surface analyzer (OSA200, Ningbo Scientific Instruments Company, China). The surface charge of the membranes was evaluated using an electrokinetic analyzer (SurPASS, Anton Paar GmbH) in a 10.0 $mmol \cdot L^{-1}$ NaCl electrolyte solution at pH 6.7 in terms of zeta potential. Specific areal electric resistance of the membranes was detected by a custom-designed four-compartment resistance analysis cell (ChemJoy Polymer Material Co., Ltd., China) in a 0.5 $mol \cdot L^{-1}$ NaCl solution, as illustrated in more detail in the Supplementary Materials. The pore size and MWCO of the membranes was measured by separation of 0.2 $g \cdot L^{-1}$ poly(ethylene glycol) solutions with various molecular weights, as detailed in the Supplementary Materials.

Pressure-driven separation performance tests

The pressure-driven separation of the coated TFC NPMs was performed using a custom-made cross-flow filtration unit at 4 bar and 25±1°C to evaluate their selectivity between the organics and the inorganic salt (i.e., NaCl) (35). Initially, the TFC NPM coupon (effective area of 22.9 cm^2) was pre-pressurized by filtering the pure water at 6 bar to achieve a steady permeate flux. Subsequently, filtration of individual pure NaCl solutions with varying concentrations (i.e., 1.0, 3.0, 7.5, and 12.0 $g \cdot L^{-1}$) or antibiotic solutions (i.e., 1.0 $g \cdot L^{-1}$ ceftriaxone sodium, cefotaxime sodium, carbenicillin disodium, or ampicillin sodium) was conducted. Finally, separation of the antibiotic/NaCl mixed solutions with different NaCl concentrations (e.g., up to 12.0 $g \cdot L^{-1}$) was conducted to evaluate the selectivity between the antibiotics and NaCl of the TFC NPMs. The rejection (R) of the solutes was calculated using Eq. 1:

$$R = \frac{C_f - C_p}{C_f} \quad (1)$$

where C_p and C_f are the concentration of antibiotics or NaCl present in the permeate and feed, respectively. The concentration of antibiotics was measured using a UV-vis spectrophotometer (Genesys^{TM} 10S UV-vis spectrophotometer, Thermo Scientific) (36-39).

The selectivity (S) between Cl^- and the antibiotics for the TFC NPMs was calculated using Eq. 2 (40):

$$S = \frac{1 - R_{NaCl}}{1 - R_{organics}} \quad (2)$$

where R_{NaCl} and $R_{organics}$ are the rejection of NaCl and antibiotics for the TFC NPMs when filtering the antibiotic/NaCl mixed solutions, respectively.

To fractionate the organics (i.e., antibiotics) and NaCl by a pressure-driven separation process, a constant-volume nanofiltration-based diafiltration using a TFC NPM (i.e., NPM-6) was conducted by a custom-designed cross-flow filtration system at 4 bar and 25±1°C (35). Specifically, a 300 mL organics/NaCl mixed solution (1.0 g·L^{-1} organics and ~ 12 g·L^{-1} NaCl) was used as feed. Pure water with various diavolume values (η, defined as the volume ratio between pure water added and the feed during diafiltration) was added into the feed at an identical rate with the permeate to keep the feed volume unchanged.

The solute rejection (R_s) of the TFC NPMs during the constant-volume nanofiltration-based diafiltration procedure was determined by Eq. 1.

The recovery rate (α) of the organics during the constant-volume nanofiltration-based diafiltration was calculated using Eq. 3:

$$\alpha = \frac{C_{final,\ organics}}{C_{initial,\ organics}} \quad (3)$$

where $C_{initial,\ organics}$ and $C_{final,\ organics}$ represent the initial and final concentration of the antibiotic in the feed, respectively.

The desalination efficiency (β) of the constant-volume nanofiltration-based diafiltration was calculated using Eq. 4:

$$\beta = 1 - \frac{C_{final,\ NaCl}}{C_{initial,\ NaCl}} \quad (4)$$

where $C_{initial,\ NaCl}$ and $C_{final,\ NaCl}$ represent the initial and final concentration of NaCl in the feed, respectively.

Electrodialytic separation performance tests

The electro-driven separation performance of the PDA/PEI coated TFC NPMs as ACMs were evaluated in a custom-designed electrodialysis cell (ChemJoy Polymer Material Co., Ltd., China), where the AEMs were replaced for anion transfer to fractionate the organics/NaCl mixed solutions (**Fig. 1B**). The electrodialysis cell consisted of a cathode, an anode, and a membrane stack (Fig. S14A), where three pieces of the CEM coupons and two pieces of the TFC NPMs (effective area of 19.4 cm^2 for each membrane coupon) were alternatively inserted. A 0.3 mol·L^{-1} Na_2SO_4 solution was used as an electrolyte in both cathode and anode chambers.

Initially, 300 mL pure NaCl solution (about 12 $g \cdot L^{-1}$) was used as the feed (diluate) in the electrodialytic separation at an applied current of 0.5 A to investigate the anion transfer capacity of the PDA/PEI coated TFC NPMs for desalination of pure NaCl solutions. The intermediate NaCl solution in the concentrate compartment had an identical salt concentration with the feed (diluate). To compare membrane performances of the surface-engineered TFC NPMs, four commercial AEMs (i.e., AEM-1, AEM-2, AEM-3 and AEM-4) were applied as ACMs in the designed electrodialytic separation cell for desalination of pure NaCl solutions. When the conductivity of the feed decreased to 0.16 $mS \cdot cm^{-1}$, the electrodialytic separation operation was stopped immediately.

The energy consumption (E) and desalination efficiency (γ) of the electrodialytic separation process was determined by Eq. 5 and Eq. 6, respectively:

$$E = \int \frac{U \cdot I \cdot \mathrm{d}t}{\left(C^{\mathrm{e}}_{\text{initial, NaCl}} - C^{\mathrm{e}}_{\text{final, NaCl}}\right) \cdot V \cdot M} \tag{5}$$

$$\gamma = 1 - \frac{C^{\mathrm{e}}_{\text{final, NaCl}}}{C^{\mathrm{e}}_{\text{initial, NaCl}}} \tag{6}$$

where U is the applied voltage, I is the applied current, M is the molar mass of NaCl, and V is the volume of the feed solution. $C^{\mathrm{e}}_{\text{initial, NaCl}}$ and $C^{\mathrm{e}}_{\text{final, NaCl}}$ represent the initial and final concentration of NaCl in the feed (diluate), respectively.

Subsequently, 300 mL antibiotic/NaCl (i.e., ceftriaxone sodium/NaCl, cefotaxine sodium/NaCl, carbenicillin disodium/NaCl or ampicillin sodium/NaCl) mixed solutions (1.0 $g \cdot L^{-1}$ antibiotic and ~ 12 $g \cdot L^{-1}$ NaCl) were further used as feed in the electrodialytic separation process using the PDA/PEI coated TFC NPMs (i.e., NPM-6) as ACMs for fractionation of antibiotics and NaCl at a current of 0.5 A. During the desalination/fractionation of the antibiotic/NaCl mixed solutions, the electrodialytic separation process was terminated as the conductivity of the feed dropped below 0.2 $mS \cdot cm^{-1}$.

Finally, the fouling propensity of the PDA/PEI coated TFC NPMs was further investigated with a six-cycle electrodialytic membrane separation operation using the ceftriaxone sodium/NaCl mixed solution as feed to verify the stability of the surface-engineered TFC NPMs (i.e., NPM-6) as ACMs for practical one-step fractionation of organics and NaCl. Additionally, the electrodialysis process equipped with the commercial AEMs (i.e., AEM-1) was conducted using the ceftriaxone sodium/NaCl mixed solution as feed in the six-cycle electrodialytic separation process under the same testing conditions, highlighting the superiority of the surface engineered TFC NPMs for fractionation of antibiotics and NaCl.

The desalination efficiency (γ) during the electrodialytic separation process for fractionation of antibiotics and NaCl was determined using Eq. 6.

The recovery rate (δ) of the antibiotics during the electrodialytic separation process for fractionation of antibiotics and NaCl was calculated using Eq. 7:

$$\delta = 1 - \frac{C^{\mathrm{e}}_{\text{final, organics}}}{C^{\mathrm{e}}_{\text{initial, organics}}} \tag{7}$$

where $C^{e}_{initial,\ organics}$ is the initial concentration of the antibiotics in the feed and $C^{e}_{final,\ organics}$ is the final concentration of the antibiotics in the concentrate compartment.

Molecular dynamics simulation

To explore the mass transport mechanism of the PDA/PEI coated TFC NPMs in electrodialysis, we simulated the transfer behavior of different ions (i.e., Cl^-, Na^+ and ampicillin ions) under an applied electric field through MD. A more detailed description of the MD simulations can be found in the Supplementary Materials.

References

1. P. L. McCarty, J. Bae, J. Kim, Domestic wastewater treatment as a net energy producer-can this be achieved? *Environ. Sci. Technol.* **45**, 7100-7106 (2011).
2. B. E. Logan, K. Rabaey, Conversion of wastes into bioelectricity and chemicals by using microbial electrochemical technologies. *Science* **337**, 686-690 (2012).
3. R. M. DuChanois, M. Heiranian, J. Yang, C. J. Porter, Q. Li, X. Zhang, R. Verduzco, M. Elimelech, Designing polymeric membranes with coordination chemistry for high-precision ion separations. *Sci. Adv.* **8**, m9436.
4. Y. Yao, P. Zhang, C. Jiang, R. M. DuChanois, X. Zhang, M. Elimelech, High performance polyester reverse osmosis desalination membrane with chlorine resistance. *Nat. Sustain.* **4**, 138-146 (2021).
5. K. Zuo, W. Wang, A. Deshmukh, S. Jia, H. Guo, R. Xin, M. Elimelech, P. M. Ajayan, J. Lou, Q. Li, Multifunctional nanocoated membranes for high-rate electrothermal desalination of hypersaline waters. *Nat. Nanotechnol.* **15**, 1025-1032 (2020).
6. J. Lin, Q. Chen, X. Huang, Z. Yan, X. Lin, W. Ye, S. Arcadio, P. Luis, J. Bi, B. Van der Bruggen, S. Zhao, Integrated loose nanofiltration-electrodialysis process for sustainable resource extraction from high-salinity textile wastewater. *J. Hazard. Mater.* **419**, 126505 (2021).
7. W. Ye, H. Liu, M. Jiang, J. Lin, K. Ye, S. Fang, Y. Xu, S. Zhao, B. Van der Bruggen, Z. He, Sustainable management of landfill leachate concentrate through recovering humic substance as liquid fertilizer by loose nanofiltration. *Water Res.* **157**, 555-563 (2019).
8. N. N. R. Ahmad, W. L. Ang, C. P. Leo, A. W. Mohammad, N. Hilal, Current advances in membrane technologies for saline wastewater treatment: A comprehensive review. *Desalination* **517**, 115170 (2021).
9. Mandeep, G. Kumar Gupta, P. Shukla, Insights into the resources generation from pulp and paper industry wastes: Challenges, perspectives and innovations. *Bioresource Technol.* **297**, 122496 (2020).
10. X. Zhang, Selective separation membranes for fractionating organics and salts for industrial wastewater treatment: Design strategies and process assessment. *J. Membr. Sci.* **643**, 120052 (2022).
11. Y. Lu, R. Wang, Y. Zhu, Z. Wang, W. Fang, S. Lin, J. Jin, Two-dimensional fractal nanocrystals templating for substantial performance enhancement of polyamide nanofiltration membrane. *Proc. Natl. Acad. Sci. U.S.A.* **118**, e2019891118 (2021).
12. Y. Liang, Y. Zhu, C. Liu, K. Lee, W. Hung, Z. Wang, Y. Li, M. Elimelech, J. Jin, S. Lin, Polyamide nanofiltration membrane with highly uniform sub-nanometre pores for sub-1 Å precision separation. *Nat. Commun.* **11**, 2015 (2020).
13. W. Zhang, H. Xu, F. Xie, X. Ma, B. Niu, M. Chen, H. Zhang, Y. Zhang, D. Long, General synthesis of ultrafine metal oxide/reduced graphene oxide nanocomposites for ultrahigh-flux nanofiltration membrane. *Nat. Commun.* **13**, 471 (2022).
14. Z. Wang, Z. Wang, S. Lin, H. Jin, S. Gao, Y. Zhu, J. Jin, Nanoparticle-templated nanofiltration membranes for ultrahigh performance desalination. *Nat. Commun.* **9**, 2004 (2018).

15. L. Shen, R. Cheng, M. Yi, W. Hung, S. Japip, L. Tian, X. Zhang, S. Jiang, S. Li, Y. Wang, Polyamide-based membranes with structural homogeneity for ultrafast molecular sieving. *Nat. Commun.* **13**, 500 (2022).
16. X. Feng, Q. Imran, Y. Zhang, L. Sixdenier, X. Lu, G. Kaufman, U. Gabinet, K. Kawabata, M. Elimelech, C. O. Osuji, Precise nanofiltration in a fouling-resistant self-assembled membrane with water-continuous transport pathways. *Sci. Adv.* **5**, v9308.
17. J. Lin, C. Y. Tang, W. Ye, S. Sun, S. H. Hamdan, A. Volodin, C. V. Haesendonck, A. Sotto, P. Luis, B. Van der Bruggen, Unraveling flux behavior of superhydrophilic loose nanofiltration membranes during textile wastewater treatment. *J. Membr. Sci.* **493**, 690-702 (2015).
18. Y. Guo, T. Li, K. Xiao, X. Wang, Y. F. Xie, Key foulants and their interactive effect in organic fouling of nanofiltration membranes. *J. Membr. Sci.* **610**, 118252 (2020).
19. S. Lee, J. Cho, M. Elimelech, Combined influence of natural organic matter (NOM) and colloidal particles on nanofiltration membrane fouling. *J. Membr. Sci.* **262**, 27-41 (2005).
20. X. Wang, C. Zhang, P. Ouyang, The possibility of separating saccharides from a NaCl solution by using nanofiltration in diafiltration mode. *J. Membr. Sci.* **204**, 271-281 (2002).
21. S. Al-Amshawee, M. Y. B. M. Yunus, A. A. M. Azoddein, D. G. Hassell, I. H. Dakhil, H. A. Hasan, Electrodialysis desalination for water and wastewater: A review. *Chem. Eng. J.* **380**, 122231 (2020).
22. T. Xu, C. Huang, Electrodialysis-based separation technologies: A critical review. *AIChE J.* **54**, 3147-3159 (2008).
23. S. K. Patel, M. Qin, W. S. Walker, M. Elimelech, Energy efficiency of electro-driven brackish water desalination: Electrodialysis significantly outperforms membrane capacitive deionization. *Environ. Sci. Technol.* **54**, 3663-3677 (2020).
24. C. Xue, Q. Chen, Y. Liu, Y. Yang, D. Xu, L. Xue, W. Zhang, Acid blue 9 desalting using electrodialysis. *J. Membr. Sci.* **493**, 28-36 (2015).
25. H. Lee, M. Hong, S. Han, S. Cho, S. Moon, Fouling of an anion exchange membrane in the electrodialysis desalination process in the presence of organic foulants. *Desalination* **238**, 60-69 (2009).
26. M. A. C. K. Hansima, M. Makehelwala, K. B. S. N. Jinadasa, Y. Wei, K. G. N. Nanayakkara, A. C. Herath, R. Weerasooriya, Fouling of ion exchange membranes used in the electrodialysis reversal advanced water treatment: A review. *Chemosphere* **263**, 127951 (2021).
27. H. Yang, R. Z. Waldman, M. Wu, J. Hou, L. Chen, S. B. Darling, Z. Xu, Dopamine: Just the right medicine for membranes. *Adv. Funct. Mater.* **28**, 1705327 (2018).
28. H. Lee, S. M. Dellatore, W. M. Miller, P. B. Messersmith, Mussel-Inspired surface chemistry for multifunctional coatings. *Science* **318**, 426-430 (2007).
29. W. Qiu, H. Yang, Z. Xu, Dopamine-assisted co-deposition: An emerging and promising strategy for surface modification. *Adv. Colloid Interfaces Sci.* **256**, 111-125 (2018).
30. F. Ponzio, J. Barthès, J. Bour, M. Michel, P. Bertani, J. Hemmerlé, M. D Ischia, V. Ball, Oxidant control of polydopamine surface chemistry in acids: A mechanism-based entry to superhydrophilic-superoleophobic coatings. *Chem. Mater.* **28**, 4697-4705 (2016).
31. M. R. Teixeira, M. J. Rosa, M. Nyström, The role of membrane charge on nanofiltration performance. *J. Membr. Sci.* **265**, 160-166 (2005).
32. A. E. Childress, M. Elimelech, Relating nanofiltration membrane performance to membrane charge (electrokinetic) characteristics. *Environ. Sci. Technol.* **34**, 3710-3716 (2000).
33. B. Jun, J. Cho, A. Jang, K. Chon, P. Westerhoff, Y. Yoon, H. Rho, Charge characteristics (surface charge vs. zeta potential) of membrane surfaces to assess the salt rejection behavior of nanofiltration membranes. *Sep. Purif. Technol.* **247**, 117026 (2020).
34. L. A. Richards, M. Vuachère, A. I. Schäfer, Impact of pH on the removal of fluoride, nitrate and boron by nanofiltration/reverse osmosis. *Desalination* **261**, 331-337 (2010).

35. J. Lin, W. Ye, H. Zeng, H. Yang, J. Shen, S. Darvishmanesh, P. Luis, A. Sotto, B. Van der Bruggen, Fractionation of direct dyes and salts in aqueous solution using loose nanofiltration membranes. *J. Membr. Sci.* **477**, 183-193 (2015).
36. J. Yang, X. Luo, Ag-doped TiO_2 immobilized cellulose-derived carbon beads: One-Pot preparation, photocatalytic degradation performance and mechanism of ceftriaxone sodium. *Appl. Surf. Sci.* **542**, 148724 (2021).
37. T. Li, P. Zhang, H. He, Z. Wang, X. Tu, D. D. Dionysiou, Highly efficient photoelectrocatalytic degradation of cefotaxime sodium on the $MoSe_2/TiO_2$ nanotubes photoanode with abundant oxygen vacancies. *J. Solid State Chem.* **303**, 122455 (2021).
38. A. Olad, R. Nosrati, Use of response surface methodology for optimization of the photocatalytic degradation of ampicillin by ZnO/polyaniline nanocomposite. *Res. Chem. Intermediat.* **41**, 1351-1363 (2015).
39. C. Lin, Y. Wang, L. Shen, C. Lin, The dentin permeability of anti-inflammatory and antibacterial drugs: In vitro study. *J. Formos. Med. Assoc.* **118**, 828-832 (2019).
40. T. Liu, H. Yuan, Q. Li, Y. Tang, Q. Zhang, W. Qian, B. Van der Bruggen, X. Wang, Ion-responsive channels of zwitterion-carbon nanotube membrane for rapid water permeation and ultrahigh mono-/multivalent ion selectivity. *ACS Nano* **9**, 7488-7496 (2015).

Acknowledgments

Funding: This work was supported by the Fujian Provincial Department of Science and Technology (2019Y0006) and the Royal Society (IEC\NSFC\211021). **Author contributions:** J.L., W.Y., M.X. and Y.M.L. conceived the idea and designed the research. J.L., W.Y., S.X., J.D., R.L., X.C., and Z.Y. prepared the PDA/PEI coated TFC NPMs and performed the pressure-driven and electro-driven separation experiments. E.Y.M.A., W.T., D.D.H. and T.Y.N. performed the MD simulation. J.L., W.Y., D.Z., S.F., D.H.S., S.Z., B.V.D.B., M.X., and Y.M.L. contributed to interpreting the data and writing the manuscript. **Competing interests:** Authors declare that they have no competing interests. **Data and materials availability:** All data needed to evaluate the conclusions in the paper are present in the paper and/or the Supplementary Materials.

Supplementary Files

This is a list of supplementary files associated with this preprint. Click to download.

- SupplementaryMaterialsnaturewater.docx
- MovieS1.mp4
- MovieS2.mp4
- MovieS3.mp4